DFT-Based Wideband Line-of-Sight MIMO Communication

Mohammad M. Mojahedian
Member, IEEE
Univ. Pompeu Fabra, Barcelona
mohammadmahdi.mojahedian@upf.edu

Masoud Attarifar
Member, IEEE
Univ. Pompeu Fabra, Barcelona
masoud.attarifar@upf.edu

Angel Lozano
Fellow, IEEE
Univ. Pompeu Fabra, Barcelona
angel.lozano@upf.edu

***Abstract*—A solution is presented to the spatial-wideband effect in line-of-sight multiple-input multiple-output transmission. This effect, which arises once the bandwidth is large enough that the propagation delay differences for distinct transmit-receive antenna pairs become comparable to the symbol period, causes frequency selectivity and intersymbol interference. The proposed solution, which only entails channel-independent DFT precoding and reception, plus delay lines, performs close to capacity for most array orientations and is compatible with both multicarrier and single-carrier signals.**

I. Introduction

Wireless systems continue their shift towards ever higher frequencies, where much idle bandwidth awaits. With 5G currently seizing mmWave bands, the attention of researchers is already moving to the subterahertz range (0.1–1 THz) [1]. Recent experiments with state-of-the-art solid-state electronics have demonstrated bit rates in excess of 100 Gb/s using 20 GHz of bandwidth at 300 GHz [2].

Besides lots of spectrum, the shift to higher frequencies offers an opportunity: the conjunction of a diminishing range and a shrinking wavelength renders multiple-input multiple-output (MIMO) transmission feasible in line-of-sight (LOS) conditions [3]–[14]. Indeed, a nonsingular channel matrix can be obtained without the need for multipath propagation, on the basis of only the array apertures, as reasonably sized arrays become large enough relative to the wavelength and the range to resolve individual antennas at the other end. This is welcome news because, given the limited diffraction and the susceptibility to blockages at these frequencies, LOS propagation is the chief transmission mechanism therein.

Although it may be tempting to think that pure LOS channels are immune to frequency selectivity and intersymbol interference (ISI), because a single propagation path connects transmitter and receiver, that is not the case. With antenna arrays in place, differences do exist among the lengths of the links for each transmit-receive antenna pair (see Fig. 1). These differences, customarily negligible, come into play at the very large bandwidths envisioned for subterahertz communication. To refer to the ensuing form of frequency selectivity, the term *spatial-wideband* has been coined [15] and, for LOS MIMO specifically, the degradation it brings about becomes pronounced for bandwidths well below 1 GHz [16], [17].

When, rather than MIMO, transmitter and receiver implement phased-array beamforming, the spatial-wideband effect manifests itself as *misfocus*, which is a drift in the focal point over frequency. (As the range grows, misfocus degenerates into *beam squint*, whereby it is only the beam direction that drifts over frequency [18]–[20].) Misfocus can be corrected with true-time-delay beamforming, where, rather than antenna-specific phase shifts, antenna-specific delays are applied to the signal (see Fig. 2) [21]–[23].

Compared with beamforming, tackling the spatial-wideband effect becomes much more challenging in LOS MIMO because, from the vantage of each receive antenna, different delays would generally have to be applied to each transmit antenna, and vice versa. A solution proposed in [16] is the one depicted in Fig. 3, which incorporates a bank of per-antenna delay lines at both transmitter and receiver; these partially equalize the link delay differences, enabling a precoder and receiver optimized for the carrier frequency to be effective over large bandwidths. Although this is a satisfying solution, it falls short of being comprehensive in two respects:

- It is least effective for near-broadside orientations, arguably the most relevant ones.
- While a single precoder and receiver are required, these are based on a singular value decomposition (SVD) of the channel at the carrier frequency. The associated computational

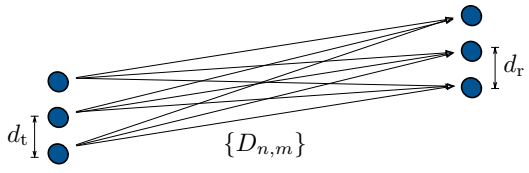

Fig. 1. Delay differences in LOS MIMO.

978-1-6654-3540-6/22 © 2022 IEEE

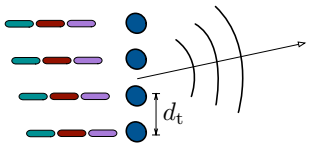

Fig. 2. True-time-delay transmit beamforming, with the stream of symbols fed into each antenna shown explicitly. The progressive delay of these streams across the array determines the beamforming direction.

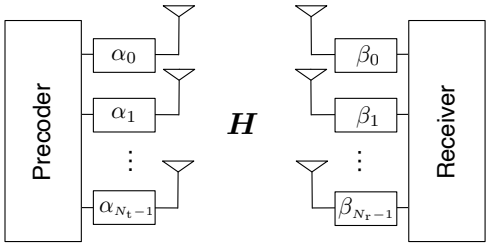

Fig. 3. MIMO with per-antenna delay lines at transmitter and receiver, plus precoding and reception tailored to the carrier frequency.

burden grows rapidly in the antenna counts.

The present paper addresses these weaknesses with a complementary approach that is most effective for orientations closer to broadside and that requires no SVDs, but only fixed DFT precoding and reception plus delay lines. The focus is on uniform linear arrays (ULAs), which experience the most severe spatial-wideband effect for given numbers of antennas.

II. Channel Model

The LOS channel under consideration is spawned by ULAs featuring N_{t} transmit and N_{r} receive antennas, with respective antenna spacings denoted by d_{t} and d_{r}. The ULA orientations can be specified in complete generality (see Fig. 4) through the corresponding elevation angles, θ_{t} and θ_{r}, plus one azimuth angle, ϕ.

The channel is regarded as static, hence known by transmitter and receiver.

A. Narrowband

Let us begin by considering a narrowband situation. Then, the channel between the mth transmit and the nth receive antenna adopts the form of the complex coefficient

$$\frac{\sqrt{G_{\mathrm{t}}G_{\mathrm{r}}}\,c}{4\pi f_{\mathrm{c}} D_{n,m}}\, e^{-j\frac{2\pi}{c}f_{\mathrm{c}}D_{n,m}} \qquad \begin{matrix} n=0,\ldots,N_{\mathrm{r}}-1 \\ m=0,\ldots,N_{\mathrm{t}}-1 \end{matrix} \tag{1}$$

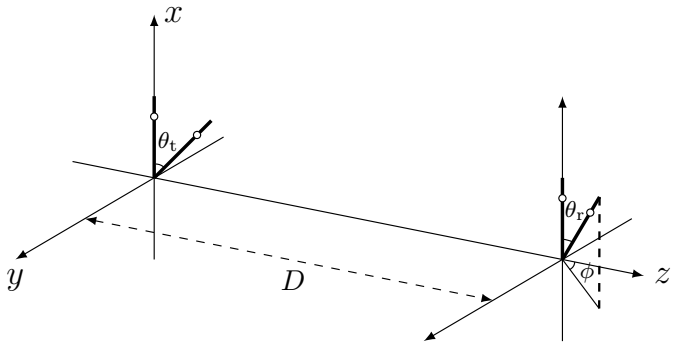

Fig. 4. LOS MIMO setting with transmit and receive ULAs.

with $D_{n,m} = \sqrt{D_x^2 + D_y^2 + D_z^2}$ the distance, given

$$D_x = nd_{\mathrm{r}}\cos\theta_{\mathrm{r}} - md_{\mathrm{t}}\cos\theta_{\mathrm{t}} \tag{2}$$

$$D_y = nd_{\mathrm{r}}\sin\theta_{\mathrm{r}}\sin\phi \tag{3}$$

$$D_z = D + nd_{\mathrm{r}}\sin\theta_{\mathrm{r}}\cos\phi - md_{\mathrm{t}}\sin\theta_{\mathrm{t}}, \tag{4}$$

and with f_{c} the carrier frequency while G_{t}, G_{r} are the antenna gains in the appropriate direction.

Provided the array apertures are small relative to $D_{n,m}$, the magnitude of (1) can be regarded as constant across n and m and the channel can be normalized into

$$\boldsymbol{H} = \begin{bmatrix} e^{-j\frac{2\pi}{c}f_{\mathrm{c}}D_{0,0}} & \ldots & e^{-j\frac{2\pi}{c}f_{\mathrm{c}}D_{0,N_{\mathrm{t}}-1}} \\ \vdots & \ddots & \vdots \\ e^{-j\frac{2\pi}{c}f_{\mathrm{c}}D_{N_{\mathrm{r}}-1,0}} & \ldots & e^{-j\frac{2\pi}{c}f_{\mathrm{c}}D_{N_{\mathrm{r}}-1,N_{\mathrm{t}}-1}} \end{bmatrix}. \tag{5}$$

Let $\boldsymbol{x} = \sqrt{\mathsf{SNR}/N_{\mathrm{t}}}\,\boldsymbol{F}\boldsymbol{s}$ be the transmit signal, with $\boldsymbol{s}$ a vector of unit-power symbols and with the precoder $\boldsymbol{F}$ satisfying $\mathrm{tr}(\boldsymbol{F}\boldsymbol{F}^*) = N_{\mathrm{t}}$ such that, given transmit power P, noise spectral density N_0, and bandwidth B,

$$\mathsf{SNR} = \frac{PG_{\mathrm{t}}G_{\mathrm{r}}c^2}{(4\pi f_{\mathrm{c}}D)^2 N_0 B} \tag{6}$$

is the signal-to-noise ratio per receive antenna. The receiver observes

$$\boldsymbol{y} = \sqrt{\frac{\mathsf{SNR}}{N_{\mathrm{t}}}}\boldsymbol{H}\boldsymbol{x} + \boldsymbol{z}, \tag{7}$$

where $\boldsymbol{z} \sim \mathcal{N}_{\mathbb{C}}(\boldsymbol{0}, \boldsymbol{I})$.

By precoding along the right singular vectors of $\boldsymbol{H}$, with powers optimized via waterfilling, while receiving along the left singular vectors, capacity can be achieved [24]. This entails the SVD of $\boldsymbol{H}$.

B. Wideband

As the bandwidth and/or the array apertures grow, the delay differences become nonnegligible relative to the symbol period

and the channel becomes frequency-selective. Then, the receiver observes

$$\mathbf{y}(f) = \sqrt{\frac{\mathsf{SNR}}{N_{\mathrm{t}}}}\mathbf{H}(f)\,\mathbf{x}(f) + \mathbf{z}(f) \qquad -\frac{B}{2} \le f \le \frac{B}{2} \tag{8}$$

where, generalizing (5), the (n,m)th entry of $\mathbf{H}(f)$ is

$$[\mathbf{H}(f)]_{n,m} = e^{-j\frac{2\pi}{c}(f_{\mathrm{c}}+f)D_{n,m}}. \tag{9}$$

If the frequency-domain pulse shape is not flat over the signal bandwidth, it can be absorbed within (9).

As, for given θ_{t} and θ_{r}, increasing ϕ can only reduce the spread of the delays, we henceforth conservatively concentrate on $\phi = 0$.

III. Information-Theoretic Capacity

Applying, now as a function of frequency, the SVD-based strategy sketched in Sec. II-A, the capacity emerges as [25]

$$C = \frac{1}{B}\sum_{k=0}^{N_{\min}-1}\int_{-B/2}^{B/2}\log_2\left(1+\mathsf{SNR}\left[\frac{1}{\gamma}-\frac{1}{\sigma_k^2(f)}\right]^+\sigma_k^2(f)\right)df \tag{10}$$

with $\sigma_k(f)$ the kth singular value of $\mathbf{H}(f)$ while γ satisfies

$$\frac{1}{B}\sum_{k=0}^{N_{\min}-1}\int_{-B/2}^{B/2}\left[\frac{1}{\gamma}-\frac{1}{\sigma_k^2(f)}\right]^+df = 1 \tag{11}$$

given $[z]^+ = \max(0,z)$. Approaching (10) entails a progressively finer partition into frequency subbands with a correspondingly exploding number of SVDs; this motivates the interest in alternative solutions that are scalable.

IV. SVD at Carrier Frequency

The solution proposed in [16] and illustrated in Fig. 3 incorporates per-antenna delay lines at transmitter and receiver, respectively $\alpha_0,\ldots,\alpha_{N_{\mathrm{t}}-1}$ and $\beta_0,\ldots,\beta_{N_{\mathrm{r}}-1}$. Although it is generally not possible to simultaneously equalize the delay differences for every transmit-receive antenna pair, by adjusting $\alpha_0,\ldots,\alpha_{N_{\mathrm{t}}-1}$ and $\beta_0,\ldots,\beta_{N_{\mathrm{r}}-1}$ so as to minimize the spread (in the mean-squared sense) of those differences, a single precoder and receiver computed from the channel SVD at the carrier frequency performs satisfactory over large bandwidths. This performance, illustrated in Figs. 8 and 9, improves as the transmit and receive arrays are rotated away from each other, being least satisfactory as their orientations become closer to broadside.

In the sequel, we present an alternative scheme that overcomes this weakness and does not entail SVDs.

V. DFT-Based Solution

When the arrays are small relative to the range D, not only is the channel magnitude constant over those arrays, but the phase is approximately quadratic thereon, such that [8]

$$\mathbf{H}(f) \approx e^{-j\frac{2\pi}{c}D(f_{\mathrm{c}}+f)}\mathbf{D}_{\mathsf{rx}}^*(f)\mathbf{H}_{\mathsf{ULA}}(f)\mathbf{D}_{\mathsf{tx}}^*(f), \tag{12}$$

where

$$[\mathbf{H}_{\mathsf{ULA}}(f)]_{n,m} = e^{j2\pi\eta(f)\frac{nm}{N_{\mathsf{max}}}} \tag{13}$$

with $N_{\mathsf{max}} = \max(N_{\mathrm{t}}, N_{\mathrm{r}})$ and

$$\eta(f) = \frac{(d_{\mathrm{r}}\cos\theta_{\mathrm{r}})(d_{\mathrm{t}}\cos\theta_{\mathrm{t}})N_{\mathsf{max}}}{cD}\,(f_{\mathrm{c}}+f). \tag{14}$$

In turn, $\mathbf{D}_{\mathsf{tx}}^*(f)$ and $\mathbf{D}_{\mathsf{rx}}^*(f)$ are diagonal matrices defined by

$$[\mathbf{D}_{\mathsf{tx}}^*(f)]_{m,m} = e^{-j\frac{2\pi}{c}\left(md_{\mathrm{t}}\sin\theta_{\mathrm{t}}+\frac{m^2}{2D}d_{\mathrm{t}}^2\right)(f_{\mathrm{c}}+f)} \tag{15}$$

$$[\mathbf{D}_{\mathsf{rx}}^*(f)]_{n,n} = e^{-j\frac{2\pi}{c}\left(nd_{\mathrm{r}}\sin\theta_{\mathrm{r}}+\frac{n^2}{2D}d_{\mathrm{r}}^2(1-\sin^2\theta_{\mathrm{r}})\right)(f_{\mathrm{c}}+f)}. \tag{16}$$

From (13), $\mathbf{H}_{\mathsf{ULA}}(f)$ is a Vandermonde matrix and, at those frequencies where $\eta(f) \le 1$, this matrix has been shown to exhibit remarkable properties that we expound next.

A. $\eta(f) \le 1$

Suppose that $\frac{N_{\mathsf{max}}}{\eta(f)}$ is integer. Then, rewriting (13) as

$$[\mathbf{H}_{\mathsf{ULA}}(f)]_{n,m} = e^{j2\pi\frac{nm}{N_{\mathsf{max}}/\eta(f)}} \tag{17}$$

we have that the $N_{\mathrm{r}}\times N_{\mathrm{t}}$ matrix $\mathbf{H}_{\mathsf{ULA}}(f)$ is a submatrix of a $\frac{N_{\mathsf{max}}}{\eta(f)}\times\frac{N_{\mathsf{max}}}{\eta(f)}$ DFT matrix. Precisely,

$$\mathbf{H}_{\mathsf{ULA}} = \sqrt{\frac{N_{\mathsf{max}}}{\eta(f)}}\begin{bmatrix}\mathbf{I}_{N_{\mathrm{r}}} & \mathbf{0}\end{bmatrix}\mathbf{\Omega}_{\frac{N_{\mathsf{max}}}{\eta(f)}}\begin{bmatrix}\mathbf{I}_{N_{\mathrm{t}}}\\ \mathbf{0}\end{bmatrix}, \tag{18}$$

where

$$[\mathbf{\Omega}_L]_{n,m} = \frac{1}{\sqrt{L}}\,e^{j2\pi\frac{nm}{L}}. \tag{19}$$

As N_{max} grows, the rounding associated with noninteger $\frac{N_{\mathsf{max}}}{\eta(f)}$ becomes immaterial and the singular values of $\mathbf{H}_{\mathsf{ULA}}$ polarize: $\eta(f)N_{\mathsf{min}}$ singular values approach a value of $\sqrt{N_{\mathsf{max}}/\eta(f)}$ while the rest vanish [26]. Moreover [8]

$$\mathbf{\Omega}_{N_{\mathrm{t}}}^*\mathbf{H}_{\mathsf{ULA}}^*(f)\mathbf{H}_{\mathsf{ULA}}(f)\mathbf{\Omega}_{N_{\mathrm{t}}} \approx \frac{N_{\mathsf{max}}}{\eta(f)}\mathrm{diag}\big(\underbrace{1,\ldots,1}_{\eta(f)N_{\mathsf{min}}},0,\ldots,0\big), \tag{20}$$

which sharpens with increasing N_{max}; thus, $\mathbf{H}_{\mathsf{ULA}}$ is asymptotically diagonalized by an $N_{\mathrm{t}}\times N_{\mathrm{t}}$ DFT matrix. It follows that, equipping the transmitter with the precoder $\mathbf{F} = \mathbf{\Omega}_{N_{\mathrm{t}}}$ plus a bank of per-antenna delays dictated by $\mathbf{D}_{\mathsf{tx}}(f)$, namely

$$\alpha_m = -\frac{1}{c}\left(md_{\mathrm{t}}\sin\theta_{\mathrm{t}}+\frac{m^2}{2D}d_{\mathrm{t}}^2\right), \tag{21}$$

the receiver observes

$$\mathbf{y}(f) = \sqrt{\frac{\mathsf{SNR}}{N_\mathrm{t}}}\,\mathbf{H}(f)\mathbf{D}_{\mathsf{tx}}(f)\mathbf{\Omega}_{N_\mathrm{t}}\mathbf{s} + \mathbf{z}(f) \tag{22}$$

and, with matched-filter combining thereon,

$$\begin{aligned}
&\Big(\mathbf{H}(f)\mathbf{D}_{\mathsf{tx}}(f)\mathbf{\Omega}_{N_\mathrm{t}}\Big)^*\mathbf{y}(f)\\
&\quad= \sqrt{\frac{\mathsf{SNR}}{N_\mathrm{t}}}\,\mathbf{\Omega}_{N_\mathrm{t}}^*\mathbf{D}_{\mathsf{tx}}(f)^*\mathbf{H}(f)^*\mathbf{H}(f)\mathbf{D}_{\mathsf{tx}}(f)\mathbf{\Omega}_{N_\mathrm{t}}\mathbf{s} + \tilde{\mathbf{z}}(f)\\
&\quad= \sqrt{\frac{\mathsf{SNR}}{N_\mathrm{t}}}\,\mathbf{\Omega}_{N_\mathrm{t}}^*\mathbf{H}(f)_{\mathsf{ULA}}^*\mathbf{H}_{\mathsf{ULA}}(f)\mathbf{\Omega}_{N_\mathrm{t}}\mathbf{s} + \tilde{\mathbf{z}}(f) &(23)\\
&\quad\approx \sqrt{\frac{\mathsf{SNR}}{N_\mathrm{t}}}\cdot\frac{N_{\mathsf{max}}}{\eta(f)}\,\mathrm{diag}\big(\underbrace{1,\ldots,1}_{\eta(f)N_{\mathsf{min}}},0,\ldots,0\big)\mathbf{s} + \tilde{\mathbf{z}}(f) &(24)
\end{aligned}$$

where the covariance of $\tilde{\mathbf{z}}(f)$ is

$$\begin{aligned}
&\mathbf{\Omega}_{N_\mathrm{t}}^*\mathbf{D}_{\mathsf{tx}}(f)^*\mathbf{H}(f)^*\mathbf{H}(f)\mathbf{D}_{\mathsf{tx}}(f)\mathbf{\Omega}_{N_\mathrm{t}} &(25)\\
&\qquad\approx \frac{N_{\mathsf{max}}}{\eta(f)}\mathrm{diag}\big(\underbrace{1,\ldots,1}_{\eta(f)N_{\mathsf{min}}},0,\ldots,0\big).
\end{aligned}$$

Altogether, we (asymptotically) obtain $\eta(f)N_{\mathsf{min}}$ parallel channels, each with signal-to-noise ratio of $\frac{N_{\mathsf{max}}}{N_\mathrm{t}}\cdot\frac{\mathsf{SNR}}{\eta(f)}$.

B. Antenna Spacings

In order to capitalize on the behavior detailed in Sec. V-A, it is necessary to guarantee that $\eta(f) \le 1$ across the entire signal bandwidth. From (14), this in turn requires that

$$d_\mathrm{t}d_\mathrm{r} \le \frac{cD}{(f_\mathrm{c}+f)\cos\theta_\mathrm{t}\cos\theta_\mathrm{r}\,N_{\mathsf{max}}}. \tag{26}$$

This condition is met, for every in-band frequency and every orientation provided that

$$d_\mathrm{t}d_\mathrm{r} \le \frac{cD}{\big(f_\mathrm{c}+\frac{B}{2}\big)N_{\mathsf{max}}}. \tag{27}$$

In the special case that $d_\mathrm{t} = d_\mathrm{r} = d$, the above explicitly gives

$$d \le \sqrt{\frac{cD}{\big(f_\mathrm{c}+\frac{B}{2}\big)N_{\mathsf{max}}}}. \tag{28}$$

Ideally, the antenna spacings should meet this condition with equality at high SNR, shrinking progressively as the SNR abates.

C. Transmit-Receive Architecture

Contingent on antenna spacings meeting the afore-specified condition, the proposed transmit-receive architecture, depicted in Fig. 5, entails

- The DFT precoder, $\mathbf{F} = \mathbf{\Omega}_{N_\mathrm{t}}$, which does not depend on the channel.
- A bank of per-antenna delay lines at the transmitter, configured as per (21).
- The matched-filter receiver $\mathbf{\Omega}_{N_\mathrm{t}}^*\mathbf{D}_{\mathsf{tx}}^*(f)\mathbf{H}(f)^*$.

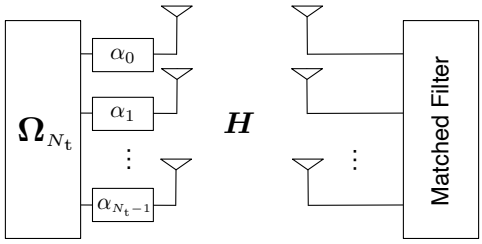

Fig. 5. Transmit-receive architecture.

This matched-filter receiver, which is frequency-selective, admits two distinct embodiments.

- With multicarrier signaling, the matched filter can be readily implemented using phase shifts on a per-subcarrier basis. The tradeoff between performance and number of subcarriers is explored in the next section.
- With either multicarrier or single-carrier signaling, the portion

$$\mathbf{D}_{\mathsf{tx}}^*(f)\mathbf{H}(f)^* \approx e^{j\frac{2\pi}{c}D(f_\mathrm{c}+f)}\mathbf{H}_{\mathsf{ULA}}^*(f)\mathbf{D}_{\mathsf{rx}}(f) \tag{29}$$

of the matched filter can be implemented via N_r banks of delay lines set to

$$\begin{aligned}
\beta_{n,m} = \frac{1}{c}\bigg(&\frac{d_\mathrm{r}\cos\theta_\mathrm{r}\,d_\mathrm{t}\cos\theta_\mathrm{t}}{D}nm &(30)\\
&- nd_\mathrm{r}\sin\theta_\mathrm{r} - \frac{n^2}{2D}d_\mathrm{r}^2(1-\sin^2\theta_\mathrm{r})\bigg)
\end{aligned}$$

with a further delay D/c, common to every m and n. These banks of delay lines, properly combined, must then be followed by the fixed DFT filter $\mathbf{\Omega}_{N_\mathrm{t}}^*$ (see Fig. 6).

VI. Performance Evaluation

For performance evaluation purposes, let us consider the situation in Fig. 7, where the transmitter is vertical ($\theta_\mathrm{t} = 0$). We further consider $N_\mathrm{t} = N_\mathrm{r} = 64$, $D = 30$ m, $f_\mathrm{c} = 300$ GHz, $B \le 20$ GHz, and the antenna spacings given by (28) taken as an equality. We hasten to emphasize that, while the formulation of the solution relies on the arrays being small relative to D, hence on (12), the results in this section are produced with the exact channel matrix.

Shown in Fig. 8 is the spectral efficiency vs θ_r. A transmission oblivious to the spatial-wideband effect performs catastrophically in most orientations. With the solution proposed in [16], the performance recovers markedly, but the shortfall from capacity is still considerable over a broad range of orientations, chiefly broadside. In contrast, the solution proposed in this paper hugs the capacity over that range. The two solutions are therefore somewhat complementary.

Fig. 9 shows the performance as the bandwidth is swept from 0.1 GHz to 20 GHz, with $\theta_\mathrm{r} = 45^\circ$. The spatial-wideband effect

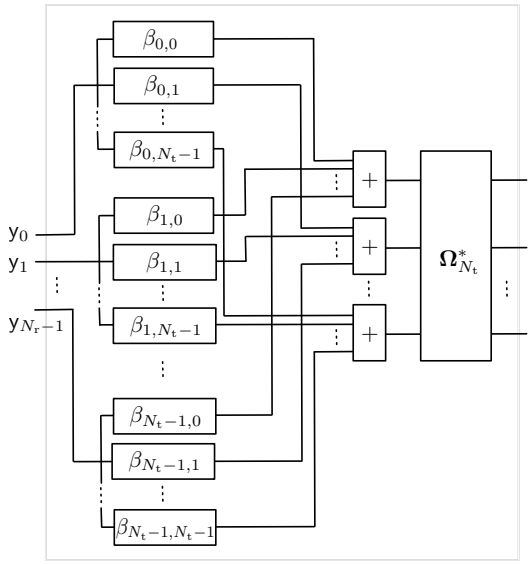

Fig. 6. Matched-filter receiver implemented as N banks of delay lines followed by a fixed DFT filter.

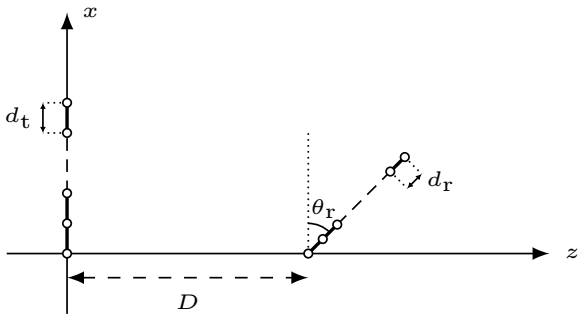

Fig. 7. Vertical transmit array with a receive array at elevation θ_r.

becomes a limiting factor for rather modest bandwidths while the performance of the proposed solution is excellent throughout, and again complementary to that of [16].

Finally, Fig. 10 contrasts the implementation based on banks of delay lines at the receiver, suitable for either multicarrier or single-carrier transmission, with an implementation specifically tailored to multicarrier signaling and based on phase shifts tuned to each subcarrier. With 64 subcarriers, corresponding to a subcarrier spacing of 312.5 MHz, the performance of the two implementations becomes almost identical. With larger subcarrier spacings, the phase-shift-based alternative begins to degrade.

VII. Summary

Equipped only with DFT precoding and reception, and per-antenna delay lines, it is possible to tightly approach the LOS MIMO capacity for most array orientations, chiefly those close

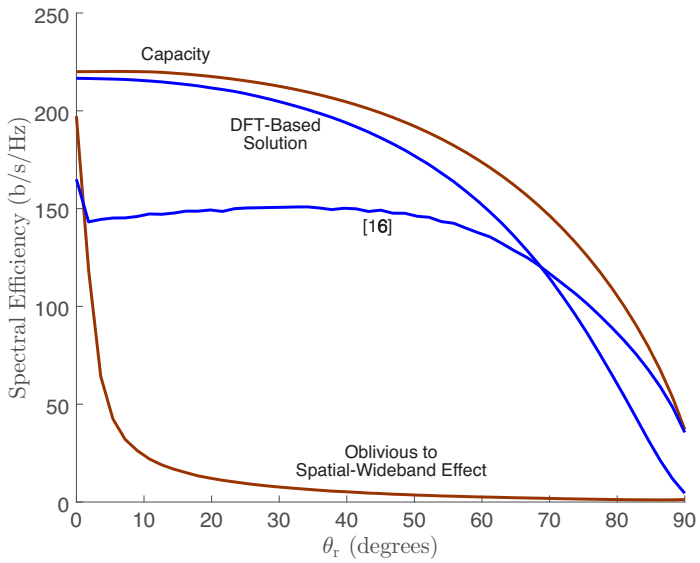

Fig. 8. Spectral efficiency vs θ_r for $N = 64$, $D = 30$ m, SNR $= 10$ dB, $f_c = 300$ GHz, and $B = 20$ GHz. Proposed DFT-based solution against the benchmark from [16], the capacity, and the performance if oblivious to the spatial-wideband effect.

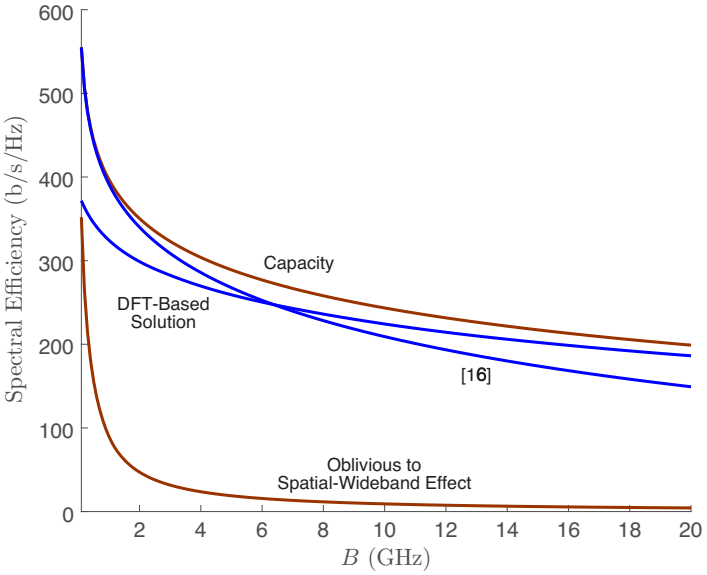

Fig. 9. Spectral efficiency vs bandwidth for $\theta_r = 45°$, $N_t = N_r = 64$, $D = 30$ m, SNR $= 10$ dB, and $f_c = 300$ GHz. Proposed DFT-based solution against the benchmark from [16], the capacity, and the performance if oblivious to the spatial-wideband effect.

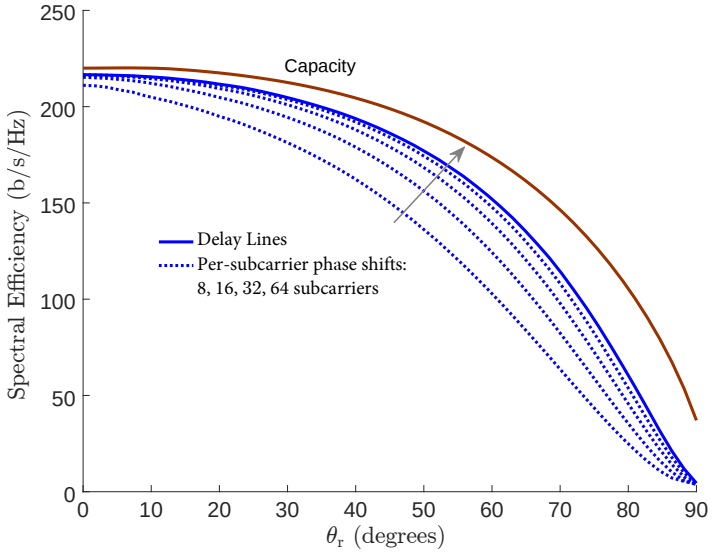

Fig. 10. Spectral efficiency vs θ_r for $N_t = N_r = 64$, $D = 30$ m, $\mathsf{SNR} = 10$ dB, $f_c = 300$ GHz, and $B = 20$ GHz. Proposed DFT-based solution implemented via banks of delay lines vs per-subcarrier phase shifts.

to broadside. Moreover, no SVDs are necessary and the solution is compatible with both multicarrier and single-carrier signaling.

Moving forward, it would be of interest to reassess the performance with estimated time-varying channels, rather than the static channels considered in this paper.

ACKNOWLEDGMENT

This work was supported by the European Research Council under the H2020 Framework Programme/ERC grant agreement 694974, by the ICREA Academia program, and by the UPF-Fractus Chair on Tech Transfer and 6G.

REFERENCES

[1] I. F. Akyildiz, J. Jornet, and C. Han, "Terahertz band: Next frontier for wireless communications," *Physical Commun.*, vol. 12, pp. 16–32, 2014.

[2] H. Hamada *et al.*, "300-GHz-band 120-Gb/s wireless front-end based on InP-HEMT PAs and mixers," *IEEE Journal of Solid-State Circuits*, vol. 55, no. 9, pp. 2316–2335, 2020.

[3] J.-S. Jiang and M. A. Ingram, "Spherical-wave model for short-range MIMO," *IEEE Trans. Commun.*, vol. 53, no. 9, pp. 1534–1541, 2005.

[4] F. Bohagen, P. Orten, and G. E. Oien, "On spherical vs. plane wave modeling of line-of-sight MIMO channels," *IEEE Trans. Commun.*, vol. 57, no. 3, pp. 841–849, 2009.

[5] M. Matthaiou, A. Sayeed, and J. A. Nossek, "Maximizing LoS MIMO capacity using reconfigurable antenna arrays," in *ITG Workshop on Smart Antennas (WSA)*, 2010, pp. 14–19.

[6] N. Chiurtu and B. Rimoldi, "Varying the antenna locations to optimize the capacity of multi-antenna Gaussian channels," in *Proc. IEEE Int. Conf. Acoust. Speech Signal Process.*, Jun. 2000, pp. 3121–3123.

[7] S. Sun, T. S. Rappaport, R. W. Heath, Jr., A. Nix, and S. Rangan, "MIMO for millimeter-wave wireless communications: Beamforming, spatial multiplexing, or both?" *IEEE Commun. Mag.*, vol. 52, no. 12, pp. 110–121, 2014.

[8] H. Do, N. Lee, and A. Lozano, "Reconfigurable ULAs for line-of-sight MIMO transmission," *IEEE Trans. Wireless Commun.*, vol. 20, no. 5, pp. 2933–2947, 2020.

[9] E. Torkildson, B. Ananthasubramaniam, U. Madhow, and M. Rodwell, "Millimeter-wave MIMO: Wireless links at optical speeds," in *Allerton Conf. Commun., Control and Computing*, 2006, pp. 1–9.

[10] E. Torkildson, U. Madhow, and M. Rodwell, "Indoor millimeter wave MIMO: Feasibility and performance," *IEEE Trans. Wireless Commun.*, vol. 10, no. 12, pp. 4150–4160, Dec. 2011.

[11] X. Song, C. Jans, L. Landau, D. Cvetkovski, and G. Fettweis, "A 60 GHz LOS MIMO backhaul design combining spatial multiplexing and beamforming for a 100 Gbps throughput," in *IEEE Global Commun. Conf.*, Dec. 2015, pp. 1–6.

[12] H. Sarieddeen, M.-S. Alouini, and T. Y. Al-Naffouri, "Terahertz-band ultra-massive spatial modulation MIMO," *IEEE J. Sel. Areas Commun.*, vol. 37, no. 9, pp. 2040–2052, 2019.

[13] C. Lin and G. Y. Li, "Terahertz communications: An array-of-subarrays solution," *IEEE Commun. Mag.*, vol. 54, no. 12, pp. 124–131, Dec. 2016.

[14] H. Do, S. Cho, J. Park, H.-J. Song, N. Lee, and A. Lozano, "Terahertz line-of-sight MIMO communication: Theory and practical challenges," *IEEE Commun. Magazine*, vol. 59, no. 3, pp. 104–109, 2021.

[15] B. Wang, F. Gao, S. Jin, H. Lin, G. Y. Li, S. Sun, and T. S. Rappaport, "Spatial-wideband effect in massive MIMO with application in mmWave systems," *IEEE Communications Magazine*, vol. 56, no. 12, pp. 134–141, 2018.

[16] M. M. Mojahedian, M. Attarifar, and A. Lozano, "Spatial-wideband effect in line-of-sight MIMO communication," in *IEEE Int'l Conf. Commun. (ICC)*, May 2022.

[17] M. Attarifar, M. Mojahedian, and A. Lozano, "Reduced-complexity wideband line-of-sight MIMO communication," in *Asilomar Conf. on Signals, Systems and Computers*, Nov. 2022.

[18] J. H. Brady and A. M. Sayeed, "Wideband communication with high-dimensional arrays: New results and transceiver architectures," in *2015 IEEE International Conference on Communication Workshop (ICCW)*. IEEE, 2015, pp. 1042–1047.

[19] B. Wang, F. Gao, S. Jin, H. Lin, and G. Y. Li, "Spatial-and frequency-wideband effects in millimeter-wave massive MIMO systems," *IEEE Transactions on Signal Processing*, vol. 66, no. 13, pp. 3393–3406, 2018.

[20] K. Dovelos, M. Matthaiou, H. Q. Ngo, and B. Bellalta, "Channel estimation and hybrid combining for wideband terahertz massive MIMO systems," *IEEE J. Sel. Areas Commun.*, vol. 39, no. 6, pp. 1604–1620, 2021.

[21] H. Hashemi, T.-S. Chu, and J. Roderick, "Integrated true-time-delay-based ultra-wideband array processing," *IEEE Commun. Mag.*, vol. 46, no. 9, pp. 162–172, 2008.

[22] P. Moosbrugger, M. Adkins, and R. Haupt, "Degradation in theoretical phase shift keying waveforms due to signal dispersion in a large communications phased array," in *IEEE Int'l Symp. Phased Array Systems and Techn.*, 2013, pp. 224–226.

[23] T.-S. Chu and H. Hashemi, "True-time-delay-based multi-beam arrays," *IEEE Trans. Microwave Theory and Techniques*, vol. 61, no. 8, pp. 3072–3082, 2013.

[24] A. Tulino, A. Lozano, and S. Verdú, "MIMO capacity with channel state information at the transmitter," in *IEEE Int'l Symp. on Spread Spectrum Techniques and Applications (ISSSTA)*, 2004, pp. 22–26.

[25] R. W. Heath, Jr. and A. Lozano, *Foundations of MIMO Communication*. Cambridge University Press, 2019.

[26] Z. Zhu, S. Karnik, M. A. Davenport, J. Romberg, and M. B. Wakin, "The eigenvalue distribution of discrete periodic time-frequency limiting operators," *IEEE Signal Process. Lett.*, vol. 25, no. 1, pp. 95–99, 2017.